Electronic Supplementary Information for

Non-Conjugated Linkage Enabling a Quinone-Based Cathode Material with Long Cycle Life and High Energy Density for Aqueous Zinc Batteries

Lu Lin,‡[a] Zhiqing Xue,‡[a] ,Tong Qiu,[a] Jiaqi Zhu,[a] Guoli Zhang,[a] Hongtu Zhan,[a] Kuo Wang[a] and Xiaoqi Sun*[ab]

[a] Department of Chemistry, Northeastern University, 3-11 Wenhua Road, Shenyang, 110819, China

[b] National Frontiers Science Center for Industrial Intelligence and Systems Optimization, Northeastern University, 3-11 Wenhua Road, Shenyang, 110819, China

‡ L. Lin and Z. Xue contributed equally to this work.

*E-mail: sunxiaoqi@mail.neu.edu.cn

Supplementary figures and table

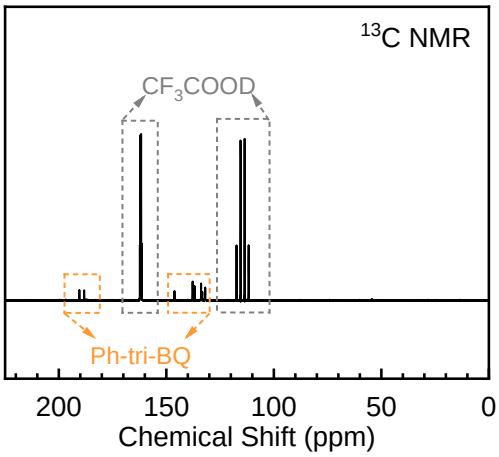

Fig. S1 ^{13}C NMR of Ph-tri-BQ (CF_3COOD solvent).

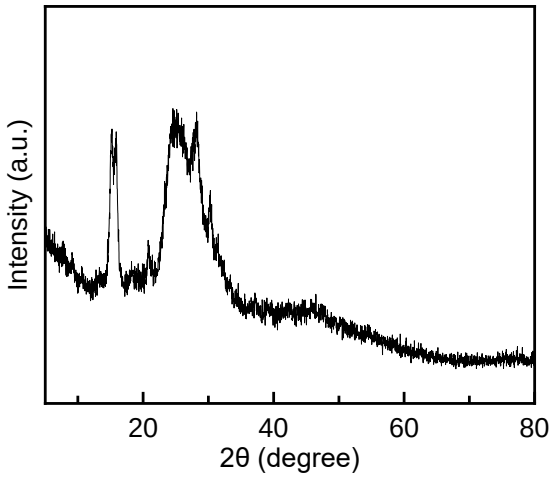

Fig. S2 XRD of Ph-tri-BQ.

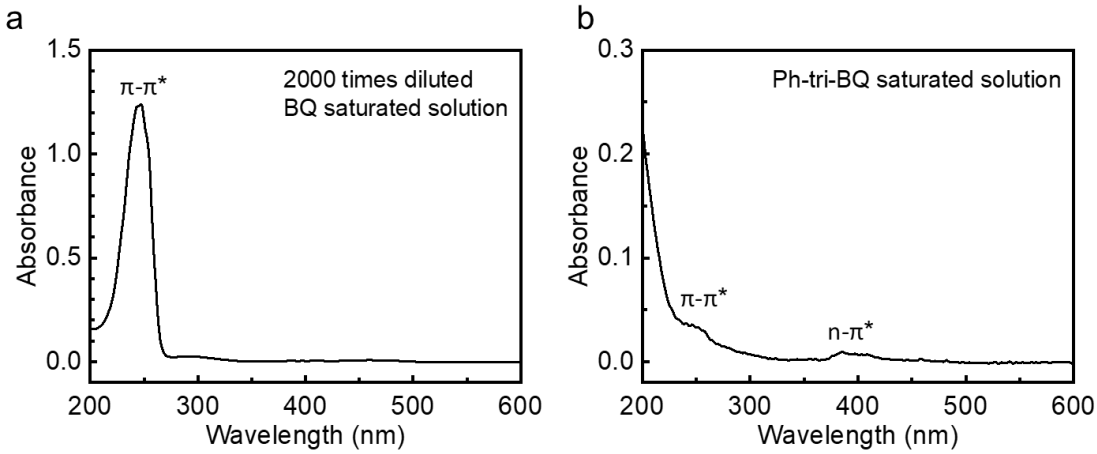

Fig. S3 The UV-Vis spectra of (a) 2000 times diluted BQ saturated solution and (b) Ph-tri-BQ saturated solution.

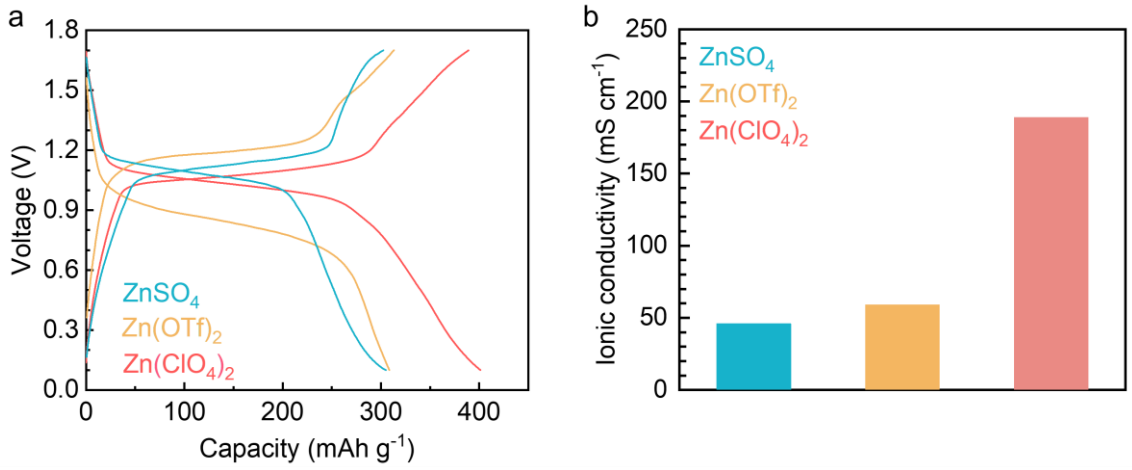

Fig. S4 (a) Charge-discharge curves of the Ph-tri-BQ cathode in the three electrolytes of 4 m $ZnSO_4$, 4 m $Zn(ClO_4)_2$, saturated $Zn(OTf)_2$ (approximately 3.5 m) and (b) the ionic conductivities of different electrolytes.

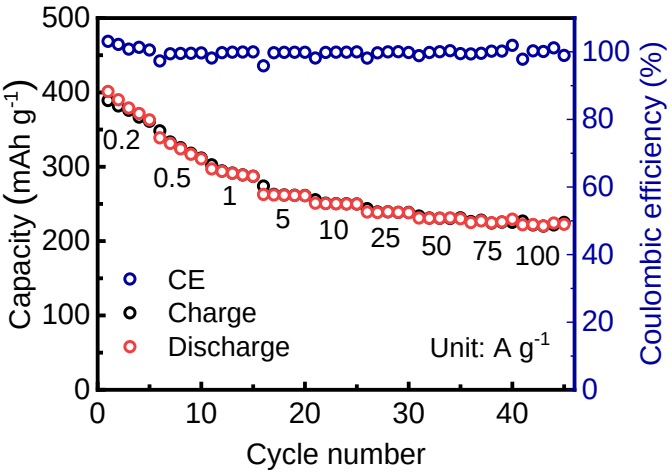

Fig. S5 Rate performance of Ph-tri-BQ at various current densities.

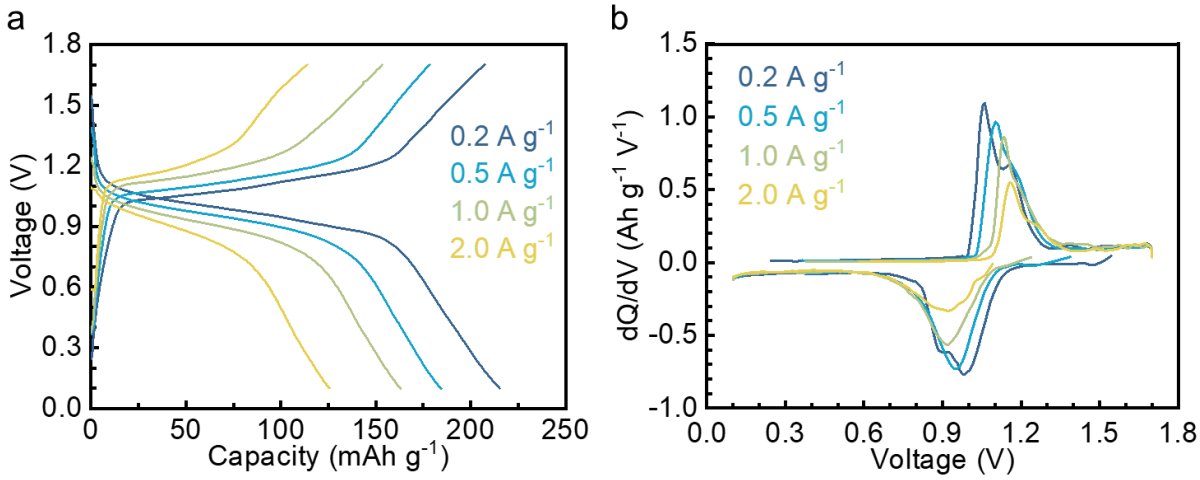

Fig. S6 (a) Charge-discharge and (b) differential capacity curves of the cathode with 80% active material at different current densities.

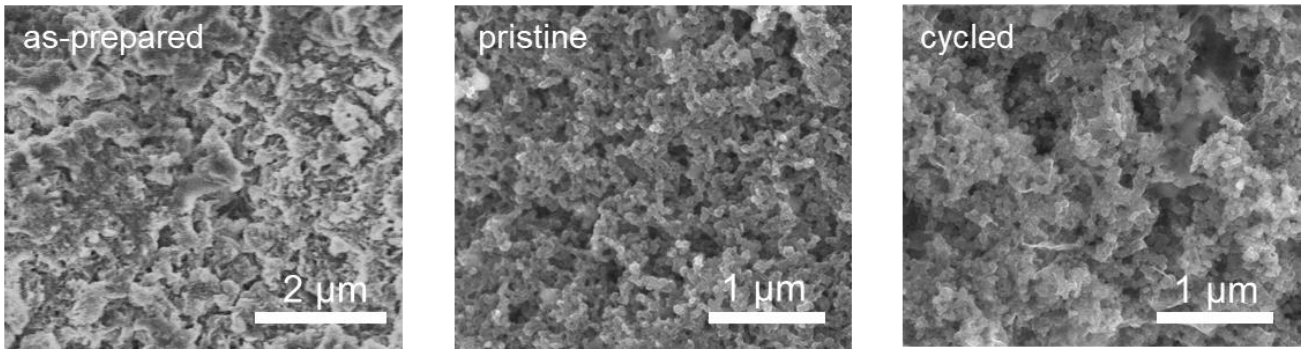

Fig. S7 SEM images of Ph-tri-BQ at different states. The as-prepared material shows the aggregation of particles. They are uniformly mixed with Ketjen Black (KB) particles in the electrode, resulting in a conductive network. After 68000 cycles at 100 A g^{-1}, the homogeneity of the materials in the electrode is preserved.

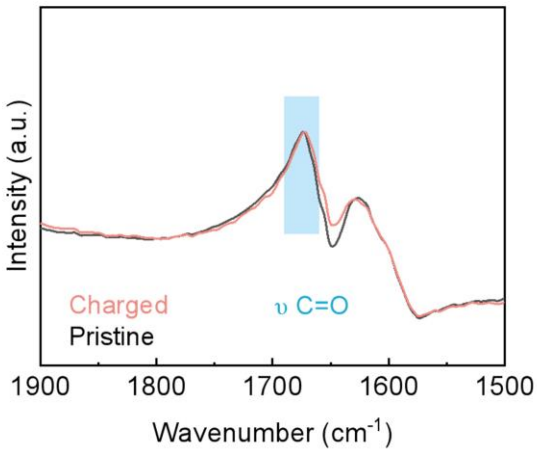

Fig. S8 ATR-FTIR spectra of the pristine and charged Ph-tri-BQ cathode.

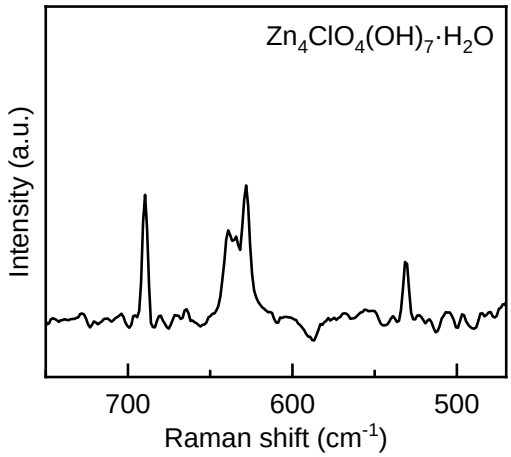

Fig. S9 Raman of the $Zn_4ClO_4(OH)_7 \cdot xH_2O$ standard.

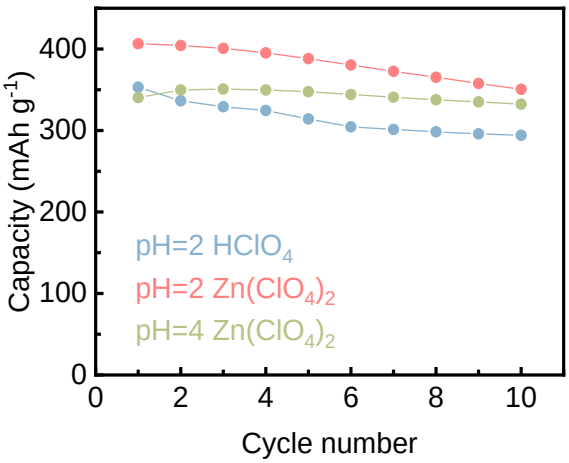

Fig. S10 The capacity evolution of Ph-tri-BQ in the three electrolytes at 0.2 A g^{-1}.

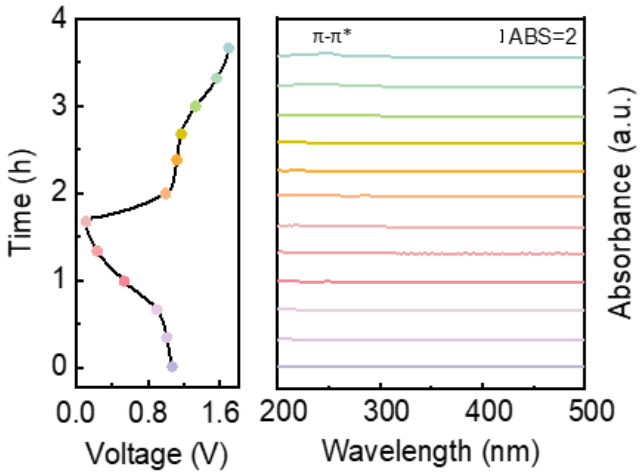

Fig. S11 In-situ UV-Vis spectra of the $Zn(ClO_4)_2$ electrolyte during the first cycle showing weak π-π* absorption peaks from Ph-tri-BQ at different states.

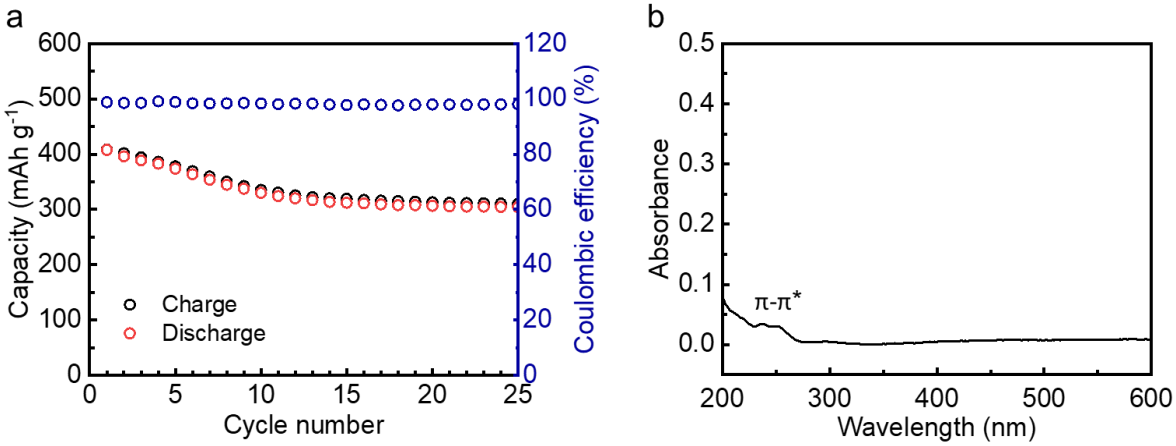

Fig. S12 (a) The capacity evolution of Ph-tri-BQ during the first 25 cycles at 0.2 A g^{-1} and (b) UV-Vis spectrum of the $Zn(ClO_4)_2$ electrolyte after 25 cycles showing weak π-π* absorption peaks from active material.

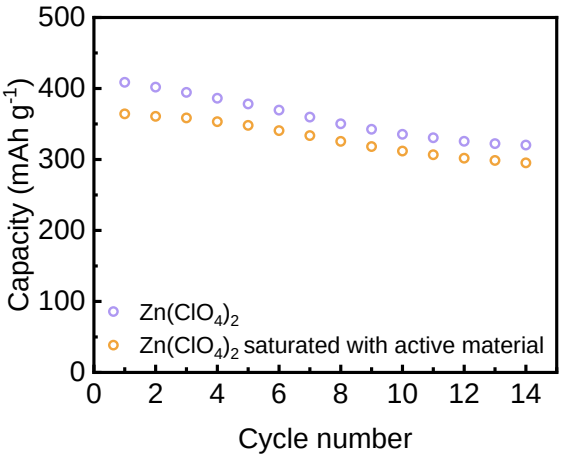

Fig. S13 The capacity evolutions of Ph-tri-BQ in the $Zn(ClO_4)_2$ electrolytes free of or saturated with active material. The same trend suggests that the low solubility of the cathode is not the primary cause of capacity drop.

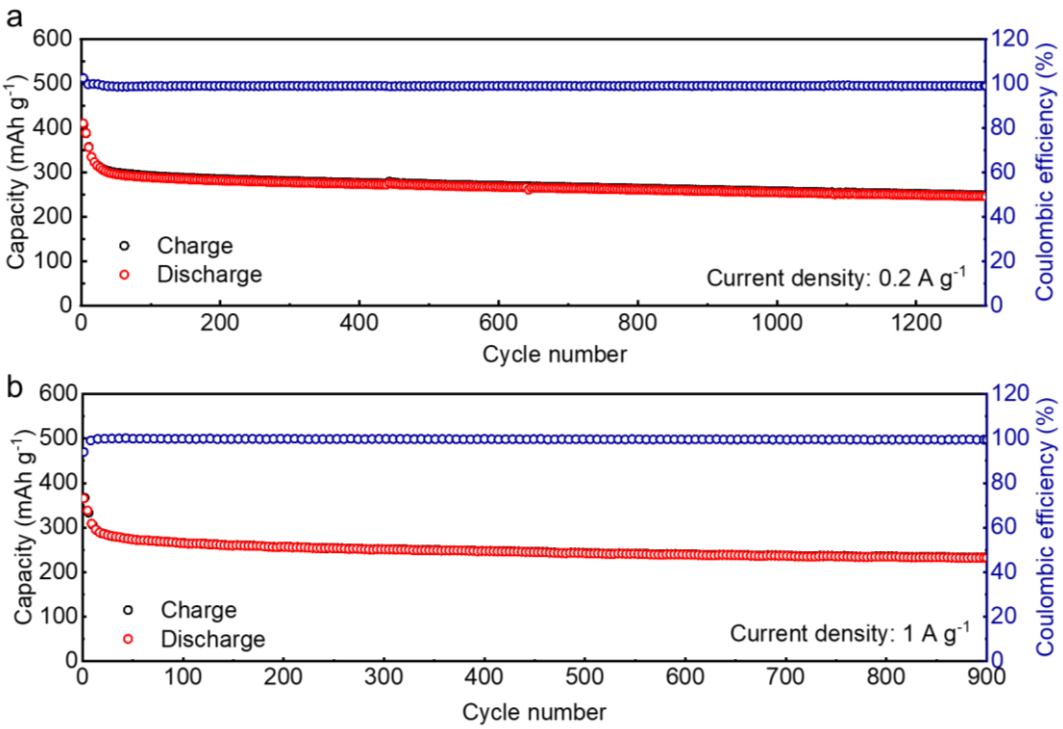

Fig. S14 Long-term cycling performance of Ph-tri-BQ at (a) 0.2 A g^{-1} and (b) 1 A g^{-1}.

Fig. S15 Digital photograph of Ph-tri-BQ.

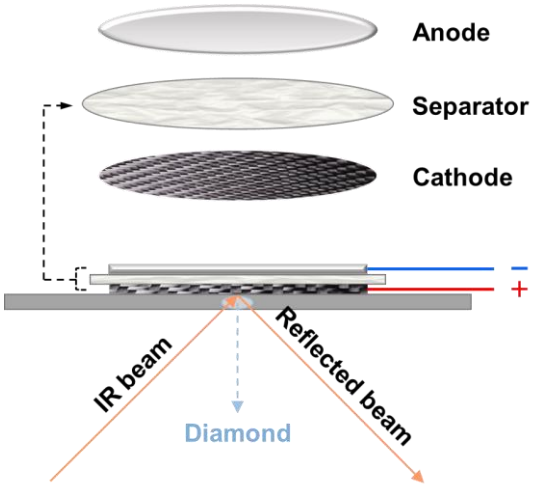

Fig. S16 Schematic diagram of in-situ ATR-FTIR analysis. The Ph-tri-BQ active material was applied on carbon cloth substrate to allow the permeation of electrolyte, and the cathode was tightly pressed on the surface of the diamond window (with active material side facing the diamond). The IR beam goes through the diamond, reaches the active material, gets reflected and travels to the detector.

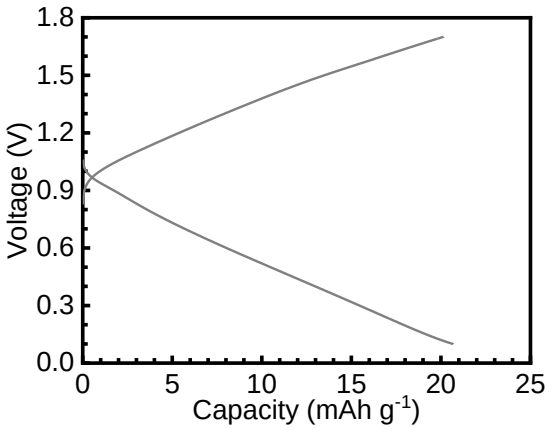

Fig. S17 The GCD curve of the electrode containing rGO, KB and PTFE without Ph-tri-BQ active material at 100 A g^{-1} (calculated based on the average mass loading of Ph-tri-BQ in electrodes).

Table S1. Theoretical elemental percentages and EA results of Ph-tri-BQ (Ph-tri-BQ·H_2O).

Element	C	H	O
Ph-tri-BQ·H_2O theoretical (wt. %)	69.57	3.38	27.05
EA (wt. %)	68.9	3.44	27.66